Leaky-Wave Analysis of TM-, TE-, and Hybrid-Polarized Aperture-Fed Bessel-Beam Launchers for Wireless-Power-Transfer Links

Edoardo Negri, *Graduate Student Member, IEEE*, Walter Fuscaldo, *Senior Member, IEEE*, Paolo Burghignoli, *Senior Member, IEEE*, and Alessandro Galli, *Member, IEEE*

***Abstract*— Bessel beams (BBs) can be generated at microwave frequencies by means of compact, planar devices based on Fabry–Perot cavity leaky-wave resonators. Most designs are based on the excitation of a single transverse magnetic/transverse electric (TM/TE) leaky mode by means of a vertical electric/magnetic dipole source. In this work, we analyze the important case of a horizontal magnetic dipole, which excites both TM and TE modes, developing an original theoretical framework suitable for resonant radiators. Analytical expressions are provided for the dominant leaky-wave aperture field. The near-field distribution is then evaluated through an accurate numerical integration of the radiating currents and validated through full-wave simulations for the relevant case of a BB launcher when excited by a waveguide-fed slot. Different designs are presented and analyzed in order to obtain TM, TE, and hybrid polarizations, finding in all cases an excellent agreement between simulations and theoretical results. Finally, we evaluate and compare the wireless-power-transfer efficiency of two coupled TM-, TE-, or hybrid-polarized BB launchers when a wireless link is established in the radiative near-field region. Interestingly, full-wave results demonstrate the superior performance of resonant BB launchers in TM or TE polarization with respect to the nonresonant hybrid case.**

***Index Terms*— Bessel beams (BBs), hybrid polarization, leaky waves, metasurfaces, wireless power transfer (WPT).**

I. Introduction

IN RECENT years, the miniaturization of devices combined with the availability of low-cost efficient sources contributed to promote microwave technology in wireless-power-transfer (WPT) applications [1]. In this frequency range, radiative WPT is way more common than nonradiative WPT, and the radiating devices are often optimized to produce directive beams in the far-field region [2]. Still, it has recently been shown in [3] and [4] that the use of focused beams in the radiative near-field region allows for reducing the waste of power, thus leading to an increased WPT efficiency. In this regard, localized beams at microwave and millimeter-wave frequencies [5], [6], [7], and in particular Bessel beams (BBs) [8], [9], have attracted much interest due to their focusing, self-healing, and limited-diffractive properties. Devices capable of radiating such beams are also known as launchers and are commonly distinguished between resonant and wideband launchers (see, e.g., [10], [11], and references therein). The former have the advantage of being compact in size, but typically show a narrow fractional bandwidth (FBW) due to their resonant nature [12], [13], [14], whereas the latter present a wideband behavior at the expense of an electrically large aperture size [15], [16], [17], [18], [19] and/or nonplanar, lens-like designs [20], [21], [22], [23], [24].

In both wideband and resonant launchers, the field polarization is commonly transverse magnetic (TM) with respect to the vertical symmetry axis of the structure. As a matter of fact, at microwave and millimeter-wave frequencies, coaxial feeders represent a very practical and low-cost choice so that they are commonly employed to excite TM-polarized BBs in the abovementioned structures. As is known, a coaxial feed source can be modeled as a vertical electric dipole (VED), which inherently excites a pure TM cylindrical wave within the launcher that, in turn, radiates a pure TM-polarized BB [12]. By duality, a pure transverse electric (TE)-polarized BB is obtained by means of a vertical magnetic dipole (VMD). This idea has indeed been exploited in [25] and [26] where loop antennas and feeding coils have been used to excite a quasi-TE-polarized BB. However, as opposed to coaxial feeders, loop antennas and feeding coils do not rigorously have azimuthal symmetry, and thus, they are not capable of exciting a pure TE-polarized BB. As shown in [26], a loop antenna feeder can properly be designed to reduce the inherent asymmetry of the source and, in turn, maximize the excitation of the H_z component and minimize the other undesired non-TE field components. Nevertheless, a pure TE-polarized BB can never be achieved; the resulting BB retains a rather hybrid polarization with a prevalent TE character.

In this regard, we should mention that TE-polarized BBs raised interest for their application in magnetic resonance imaging scenarios [27], where it is important to focus the H_z component at considerably low frequencies (namely in the range of few tens of megahertz [28]).

Manuscript received 15 July 2022; revised 5 November 2022; accepted 26 November 2022. Date of publication 27 December 2022; date of current version 3 February 2023. This work was supported by the Ministero dell'Università e della Ricerca under Grant PRIN n. 2017YJE9XK. *(Corresponding author: Edoardo Negri.)*

Edoardo Negri, Paolo Burghignoli, and Alessandro Galli are with the Department of Information Engineering, Electronics and Telecommunications, Sapienza University of Rome, 00184 Rome, Italy (e-mail: edoardo.negri@uniroma1.it).

Walter Fuscaldo is with the Istituto per la Microelettronica e Microsistemi, Consiglio Nazionale delle Ricerche, 00133 Rome, Italy.

Color versions of one or more figures in this article are available at https://doi.org/10.1109/TAP.2022.3231086.

Digital Object Identifier 10.1109/TAP.2022.3231086

Furthermore, there also exist experimental realizations of BBs whose polarization is neither TM nor TE, but hybrid (see, e.g., [19], [29], [30]). As commented in [29], BBs with transverse linear polarization (which is a type of hybrid polarization) can maintain their polarization over a "large" propagation distance when reflected, a feature particularly attractive in detection systems [31]. Despite the interest that hybrid-polarized BBs can raise in many practical applications, there is still no theoretical framework that allows for an approximate analytical treatment of the near-field distributions radiated by resonant BB launchers when excited by a source that is neither purely TM nor purely TE. In [32], all possible polarization cases have rigorously been described through a vector angular spectrum decomposition; however, this approach does not account for the resonant character of the cavity and assumes the field distribution to be directly imposed over the radiating aperture.

In this work, we aim at providing a simple, yet rigorous theoretical framework that allows for accurately describing the near-field distributions of the electromagnetic fields radiated by a BB launcher when excited by a horizontal dipole. The latter can model realistic sources in the microwave and millimeter-wave range such as waveguide-fed resonant slots etched in the ground plane or patch antenna feeders, as well as in the terahertz (THz) range, such as a slot in the ground plane back-illuminated by a collimated THz beam [33]. In this regard, we should stress that at THz frequencies, hybrid-polarized BBs become more common than TM-polarized BBs due to the unavailability of commercial coaxial cables at frequencies beyond about 110 GHz. This aspect makes even more important to establish a theoretical framework for the analysis of BB launchers excited by a waveguide-fed slot and with different polarizations.

For this kind of structure, we will show here that it is possible to choose a TM or TE polarization by enforcing different radial resonances with different aperture-radius values. In the absence of the TM or TE radial resonance, a hybrid polarization is excited for which neither TM nor TE components are negligible.

This article is organized as follows. We show in Section II, by means of a leaky-wave analysis, that it is possible to correctly predict the radiated near-field distributions of all components by describing the aperture field as a superposition of a purely TM and a purely TE cylindrical wave. We assume that the total aperture field is dominated by the leaky-wave aperture field: an assumption that will be proven consistent through full-wave simulations. For both polarizations, an outward traveling and a standing cylindrical leaky wave are considered: the former describes the field excited by the source, whereas the latter considers the reflection effect of the metallic rim of the launcher. We show in Section III that, in particular, the coefficients of the outward contributions can easily be computed from the residues of the 1-D Green's function of the relevant transverse equivalent network (TEN). Fully analytical expressions are thus provided for the aperture fields; then, the near-field distributions are obtained either analytically by assuming the nondiffractive behavior of the resulting beams or numerically by using the Huygens–Fresnel radiation integral. Numerical results are validated in Section IV with full-wave simulations. Two case studies are finally shown in Section V to assess the effectiveness of BB launchers excited by waveguide-fed slot on the ground plane in WPT scenarios (in Section V-A) and to compare their performance with a typical nonradiative near-field WPT link (in Section V-B). Conclusions are drawn in Section VI.

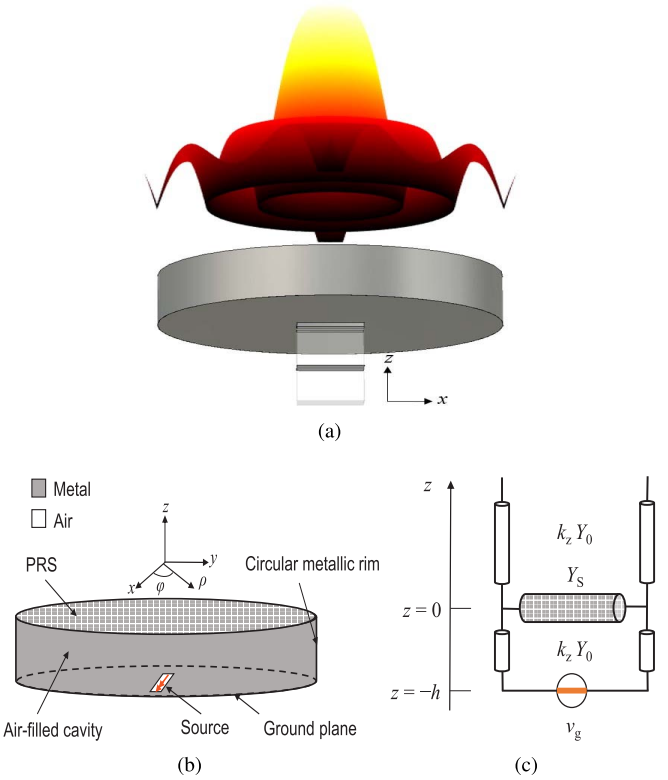

Fig. 1. (a) Pictorial representation of a BB launcher excited by a slot with the $|E_y|$ distribution, normalized with respect to its maximum and represented through a colormap from black (−30 dB) to white (0 dB), on the xz plane over the aperture. (b) Schematic view of a BB launcher centrally fed by an etched slot. (c) TEN associated with TM or TE waves supported by the structure.

II. Theoretical Approach

We obtain here an analytical description of a BB launcher excited by a horizontal magnetic dipole (HMD) that can model, e.g., a waveguide-fed slot etched in the ground plane [see Fig. 1(a)]. In this case, both TE and TM polarizations are excited, and thus, the HMD generates a hybrid-polarized electromagnetic field. Although the analysis is reported for an HMD excitation, it can be extended by duality to the case of a properly located horizontal electric dipole (HED), which is thus not repeated for brevity.

Regardless of the polarization type, the geometrical structure of the BB launcher is azimuthally invariant, being characterized by a circular grounded dielectric slab of height h enclosed by a circular metallic rim of radius ρ_{ap}, and with a lossless partially reflecting surface (PRS) on top, excited by a simple dipole-like source at the center, as shown in Fig. 1(b). In the following, we will always deal with air-filled cavities, and isotropic lossless PRS although the extension

to the dielectric-filled case and anisotropic lossy PRS is straightforward. The first assumption allows us to assume the same parameters inside and outside the cavity in the equivalent circuit of the device [see Fig. 1(c)]. The second assumption allows to fully describe the electromagnetic properties of the PRS with a single scalar purely imaginary admittance sheet $Y_s = jB_s$, which can be either inductive ($B_s < 0$) or capacitive ($B_s > 0$). A partially open parallel-plate waveguide is thus formed, of the same kind of those used in Fabry–Perot cavity antennas, which can support leaky waves [34].

In general, as shown in [35], for an HMD aligned along, e.g., the x-axis [see Fig. 1(b)], the vertical z-component of the magnetic vector potential $\mathbf{A}$ has a $\sin\phi$ variation along the azimuthal plane. Although in principle, cylindrical waves with higher order ϕ variation could be treated (see, e.g., [36], [37], [38]), the $n = 0$ (for the cases with azimuthal symmetry) and $n = 1$ modes are the most important since elementary electric and magnetic dipoles within layered media will excite only these wave types [35]. An HMD excites both TE and TM waves that can initially be studied separately and then added together.

We start from the TM case described by the magnetic vector potential $\mathbf{A} = A_z\mathbf{z}_0$. As shown in [35] and [36], for a TM cylindrical leaky wave in a grounded planar waveguide with $n = 1$, one has, in the air region $z \geq 0$ above the PRS

$$\mathbf{A} = C_{1e}Q_0H_1^{(2)}\left(k_{\rho e}\rho\right)e^{-jk_{ze}z}\sin\phi\mathbf{z_0} \tag{1}$$

where $k_{\rho e}$ and $k_{ze} = \sqrt{k_0^2 - k_{\rho e}^2}$ are the complex, TM leaky radial and longitudinal wavenumbers, respectively (k_0 is the free-space wavenumber), $H_1^{(2)}(\cdot)$ is the first-order Hankel function of the second kind, $Q_0[\mathrm{V}\cdot\mathrm{m}]$ is the complex amplitude coefficient of the HMD, C_{1e} depends on the physical and geometrical parameters of the structure (as we will thoroughly discuss in Section III), and the subscript "e" (and next the subscript "h") represents the TM-polarized (and TE-polarized) case of each quantity. In the following, we let $A_0 = C_{1e}Q_0$ [A] for the sake of conciseness.

As opposed to the infinitely extended case proposed in [35] and [36], the vector potential of a BB launcher needs also a first-order Bessel function of the first kind $J_1(\cdot)$ in order to correctly describe the scattered field on the circular metallic rim through a potential contribution that is regular at $\rho = 0$. Therefore, the magnetic vector potential reads

$$\mathbf{A} = \mathcal{C}_A(\rho)e^{-jk_{ze}z}\sin\phi\mathbf{z_0} \tag{2}$$

where $\mathcal{C}_A(\rho)$ describes the radial dependence as follows:

$$\mathcal{C}_A(\rho) = A_0H_1^{(2)}\left(k_{\rho e}\rho\right) + B_{0e}J_1\left(k_{\rho e}\rho\right) \tag{3}$$

being B_{0e} the complex amplitude coefficient of the stationary part of the magnetic vector potential. From (2), the TM field components take the following form:

$$H_\rho = \frac{\mathcal{C}_A(\rho)}{\rho}\cos\phi\, e^{-jk_{ze}z} \tag{4a}$$

$$H_\phi = -k_{\rho e}\mathcal{C}_A'(\rho)\sin\phi e^{-jk_{ze}z} \tag{4b}$$

$$H_z = 0 \tag{4c}$$

$$E_\rho = -\frac{k_{ze}k_{\rho e}}{\omega\varepsilon_0}\mathcal{C}_A'(\rho)\sin\phi\, e^{-jk_{ze}z} \tag{4d}$$

$$E_\phi = -\frac{k_{ze}}{\omega\varepsilon_0\rho}\mathcal{C}_A(\rho)\cos\phi\, e^{-jk_{ze}z} \tag{4e}$$

$$E_z = \frac{k_{\rho e}^2}{j\omega\varepsilon_0}\mathcal{C}_A(\rho)\sin\phi\, e^{-jk_{ze}z} \tag{4f}$$

where the "prime" represents the first derivative with respect to ρ.

By duality, the TE case is represented by a vector electric potential with a $\cos\phi$ variation along the azimuthal plane and the following form:

$$\mathbf{F} = \mathcal{C}_F(\rho)e^{-jk_{zh}z}\cos\phi\mathbf{z_0} \tag{5}$$

where $\mathcal{C}_F(\rho)$ reads

$$\mathcal{C}_F(\rho) = F_0H_1^{(2)}\left(k_{\rho h}\rho\right) + B_{0h}J_1\left(k_{\rho h}\rho\right) \tag{6}$$

being $F_0 = C_{1h}Q_0$ [V], C_{1h}, and B_{0h} the TE counterparts of A_0, C_{1e}, and B_{0e} for the TM case, respectively (the $C_{1e,h}$ coefficients will be commented in Section III). As for the TM case, the TE field components follow from (5) and take the following expressions:

$$E_\rho = \frac{\mathcal{C}_F(\rho)}{\rho}\sin\phi\, e^{-jk_{zh}z} \tag{7a}$$

$$E_\phi = k_{\rho h}\mathcal{C}_F'(\rho)\cos\phi\, e^{-jk_{zh}z} \tag{7b}$$

$$E_z = 0 \tag{7c}$$

$$H_\rho = -\frac{k_{\rho h}k_{zh}}{\omega\mu_0}\mathcal{C}_F'(\rho)\cos\phi\, e^{-jk_{zh}z} \tag{7d}$$

$$H_\phi = \frac{k_{zh}}{\omega\mu_0\rho}\mathcal{C}_F(\rho)\sin\phi\, e^{-jk_{zh}z} \tag{7e}$$

$$H_z = \frac{k_{\rho h}^2}{j\omega\mu_0}\mathcal{C}_F(\rho)\cos\phi\, e^{-jk_{zh}z}. \tag{7f}$$

In order to obtain the correct overall leaky-wave aperture-field distribution of a launcher excited by an ideal HMD, the complex coefficients A_0 and F_0 have first to be properly found before the expressions in (4a)–(4f) and (7a)–(7f) can be added together. The determination of A_0 and F_0 requires a residue analysis of the relevant 1-D Green's function of the structure in the spectral domain, which is addressed in Section III. These coefficients are indeed related to the outward cylindrical leaky-wave contribution to the total field excited in the infinite structure over the xy plane, but their simple evaluation does not consider the resonant character of the device. The latter, which is better described by a standing-wave solution given by the $J_1(\cdot)$ contributions of $\mathcal{C}(\rho)$, is nonnegligible and can also be the dominant contribution, as shown later.

While the coefficients of the outward leaky wave are evaluated through a residue analysis, B_{0e} and B_{0h} are found by applying the boundary condition on the circular metallic rim. In TM polarization, the radial dependence of the tangential electric field at the circular metallic rim is the same of the magnetic vector potential [see (4e) and (4f)]. Thus, applying the boundary condition at the rim location $\rho = \rho_{\mathrm{ap}}$, we obtain

$$B_{0e} = -\frac{A_0H_1^{(2)}\left(k_{\rho e}\rho_{\mathrm{ap}}\right)}{J_1\left(k_{\rho e}\rho_{\mathrm{ap}}\right)}. \tag{8}$$

In the TE case, instead, the radial dependence of the tangential electric field on the circular metallic rim is given by the first derivative of F_z with respect to ρ [see (7b)]. By the same token, an equation similar to (8) is found and reads

$$B_{0h} = -\frac{F_0 H_1'^{(2)}\left(k_{\rho h}\rho_{\mathrm{ap}}\right)}{J_1'\left(k_{\rho h}\rho_{\mathrm{ap}}\right)}. \tag{9}$$

As shown in (8) and (9), the excitation coefficients of the TM and TE resonant parts of the field are proportional to both A_0 and F_0 through a correction factor that considers the radial resonance of the structure. Therefore, the total leaky-wave aperture field can be obtained by a weighted superposition of the TE and TM leaky-wave fields.

The resonant contribution is dominant when the aperture-radius value is set to enforce a radial resonance between the outward cylindrical leaky wave launched by the central feeder and the inward one coming from reflection due to the circular metallic rim [12]. In particular, as we will thoroughly discuss in Section IV, a TM or TE radial resonance is achieved when the product $\beta\rho_{\mathrm{ap}}$ is, respectively, set equal to one of the zeros of $J_1(\cdot)$ or $J_1'(\cdot)$ in order to obtain a stationary field distribution, where β represents the phase constant of the generally complex, leaky, radial wavenumber $k_\rho = \beta - j\alpha$ (being α the so-called attenuation constant or leakage rate). By enforcing a TM or TE radial resonance with a Bessel-like field distribution, due to the limited-diffraction behavior of BBs, we can assume an invariant aperture field at each z-plane for $0 \le z \le z_{\mathrm{ndr}}$, being $z = 0$ the aperture plane and z_{ndr} the so-called nondiffractive range [12]. We recall here that for truncated BBs, the nondiffractive range takes the following approximate expression:

$$z_{\mathrm{ndr}} = \rho_{\mathrm{ap}} \cot\theta_0 \tag{10}$$

where θ_0 is the so-called axicon angle (evaluated with respect to the vertical z-axis) that can be found through the relation $\beta = k_0 \sin\theta_0$, regardless of the polarization type of the launcher. In addition, when BBs are generated through leaky waves [39], and the effective nondiffractive range is reduced in amounts that depend on the leakage rate (see [40, eq. (4)]). In the cases treated here, as is customary for such devices, the leakage rate is assumed to be small enough not to affect the nondiffractive range of a truncated BB. It is worthwhile noting that, when the radial resonance of the TE or TM field is enforced, the resonant polarization and the resonant part of the field distribution (given by the $J_1(\cdot)$ components in the relevant vector potential) become dominant. Therefore, the contribution of the nonresonant polarization is negligible and the residue evaluation is no more needed for evaluating the near-field distribution.

On the other hand, for a nonresonant design producing a hybrid polarization, the spatial distribution of the resonant part of the total aperture fields depends on the ratio between the TE and TM excitation coefficients. Such a ratio is a product of two terms for the resonant part of the field distribution: one that only depends on the residues (i.e., C_{1h} and C_{1e} or, equivalently, A_0 and F_0) and a correction factor that considers the boundary condition on the rim

$$\frac{B_{0h}}{B_{0e}} = \frac{C_{1h}}{C_{1e}} \frac{H_1'^{(2)}\left(k_{\rho h}\rho_{\mathrm{ap}}\right) J_1\left(k_{\rho e}\rho_{\mathrm{ap}}\right)}{J_1'\left(k_{\rho h}\rho_{\mathrm{ap}}\right) H_1^{(2)}\left(k_{\rho e}\rho_{\mathrm{ap}}\right)}. \tag{11}$$

As already mentioned, by enforcing a TM/TE radial resonance, the field distributions can be obtained from a vector potential proportional to $J_1(k_{\rho e,h}\rho)$ and the coefficient in (11) tends to zero/infinity (recall that the TM and TE radial resonances enforce a zero in the $J_1(\cdot)$ and $J_1'(\cdot)$ distributions, respectively).

III. Residue Evaluation

In this section, we show how A_0 and F_0 are evaluated. Assuming that without loss of generality, $Q_0 = 1$ [V · m], the vector-potential coefficients can totally be described computing C_{1e} and C_{1h}. The latter quantities are strictly related to the residues of the 1-D spectral Green's functions of the structure at the relevant leaky poles. In order to find the values of the residues, we have modeled the structure under the invariance approximation along the xy plane considering its TEN for both TE and TM cases, as shown in Fig. 1(c). Using the transverse resonance technique on the TEN for both polarizations, the dispersion equation can be expressed as

$$Y_{0e,h} + Y_{\mathrm{s}} - jY_{0e,h}\cot\left(k_{ze,h}h\right) = 0 \tag{12}$$

where $Y_{0e} = k_0/(k_{ze}\zeta_0)$ and $Y_{0h} = k_{zh}/(k_0\zeta_0)$ are, respectively, the TM and TE characteristic admittances of the transmission-line sections, in which ζ_0 is the free-space impedance. Numerically solving (12) in the complex plane, dispersion curves can be found for both TE polarization and TM polarization.

As shown in [36], C_{1e} and C_{1h} are proportional to the residues of the current and voltage at the interface ($z = 0$) of the TEN of the structure [see Fig. 1(c)]. More precisely, we can write

$$C_{1e} = \frac{j}{2}\mathrm{Res}\left\{\hat{I}_{ve}, k_\rho = k_{\rho e}\right\} \tag{13}$$

$$C_{1h} = -\frac{j}{2}\mathrm{Res}\left\{\hat{V}_{vh}, k_\rho = k_{\rho h}\right\} \tag{14}$$

where the subscript "v" stands for the voltage type of the generator v_{g}, which represents the HMD located on the ground plane. The network Green's functions $\hat{I}_{ve}$ and $\hat{V}_{vh}$ in (13) and (14) are calculated by means of a standard transmission-line approach applied to the TEN of the structure assuming unitary v_g. The resulting expressions read

$$\hat{V}_{vh} = \frac{jk_z}{\left(k_z + k_0\bar{Y}_{\mathrm{s}}\right)\sin(k_z h) - jk_z\cos(k_z h)} \tag{15}$$

$$\hat{I}_{ve} = \frac{jk_0^2}{\zeta_0\left[\left(k_z k_0 + k_z^2\bar{Y}_{\mathrm{s}}\right)\sin(k_z h) - jk_z k_0\cos(k_z h)\right]} \tag{16}$$

where $\bar{Y}_{\mathrm{s}} = \zeta_0 Y_{\mathrm{s}}$ is the normalized admittance of the PRS.

Due to the rational form of (15) and (16) (see, e.g., [41]) and assuming that the spectral Green's functions have simple poles at the leaky wavenumbers, the residues can simply be evaluated as

$$\mathrm{Res}\left\{f\left(k_\rho\right)\right\} = \frac{\widetilde{N}}{\frac{\partial\widetilde{D}}{\partial k_\rho}} \tag{17}$$

where $\widetilde{N}$ and $\widetilde{D}$ are the numerator and denominator of a rational function $f(k_\rho)$ that can represent $\hat{I}_{ve}$ for $k_\rho = k_{\rho e}$ or $\hat{V}_{vh}$ for $k_\rho = k_{\rho h}$, respectively.

Since the PRS is assumed spatially nondispersive and, hence, $\bar{Y}_\mathrm{s}$ is independent of k_z, and $\partial k_z/\partial k_\rho = -k_\rho/k_z$, we can analytically find the residues as follows:

$$C_{1e} = k_0^2 k_{ze}\Big\{2k_{\rho e}\zeta_0\Big[\sin(k_{ze}h)\big(k_0 + 2k_{ze}\bar{Y}_\mathrm{s} + jk_{ze}k_0h\big) + \cos(k_{ze}h)\big(hk_0k_{ze} + k_{ze}^2h\bar{Y}_\mathrm{s} - jk_0\big)\Big]\Big\}^{-1} \tag{18}$$

$$C_{1h} = -k_{zh}^2\Big\{2k_{\rho h}\Big[\sin(k_{zh}h)(1 + jk_{zh}h) + \cos(k_{zh}h)\big(k_{zh}h + k_0\bar{Y}_\mathrm{s}h - j\big)\Big]\Big\}^{-1}. \tag{19}$$

IV. Results

In Sections II and III, we have shown how the aperture-field distribution of a BB launcher, excited by an HMD aligned along the x-axis, can theoretically be found. In a zeroth-order approximation of ideal, diffraction-free propagation, such an aperture field can be used to represent the near field within the nondiffracting range given by (10). More accurate results with respect to this aperture-field approximation can be obtained by using the Huygens–Fresnel radiation integral. These results (hereafter referred to as "radiation-integral results") are then corroborated through full-wave simulations (in CST Microwave Studio [42]) of the 3-D structure shown in Fig. 1(a). In this section, in particular, we show some relevant designs of an HMD-fed BB launcher at the working frequency $f_0 = 30$ GHz and, then, we make a comparison between the field generated by the full-wave simulation and the radiation-integral results.

As a reference case, we analyze a BB launcher excited by a standard rectangular waveguide through a slot etched in the ground plane [see Fig. 1(a)]. The rectangular waveguide has lateral dimensions $\lambda/3$ and $2\lambda/3$ in order to have only the fundamental TE_{10} mode under propagation. As is well known, this kind of feeder acts similarly to an ideal HMD that excites both the TE and TM modes supported by the cavity. These partially guided modes can be seen as those of a Fabry–Perot cavity with a PRS printed on top. In the full-wave simulations, we have modeled the PRS as a two-sided surface impedance boundary condition (SIBC) with a frequency dispersion that respects Foster's reactance theorem [43]. Therefore, for the inductive PRS considered in this work, $X_\mathrm{S} = 2\pi f L$ has been used by fixing the lumped inductance L so as to match the desired value of X_S at the working frequency f_0. It is worthwhile to point out that the representation of a realistic isotropic PRS through the SIBC in a full-wave solver can some how differ from the exact implementation of the structure, yet it produces sufficiently accurate results to corroborate the concept (see, e.g., [12]). In particular, common geometries, such as 2-D patch arrays, strip gratings, and fishnet-like metasurfaces, can accurately be described in this way and properly designed in order to have the desired X_S value [44], [45].

The cavity height h is set to $h \simeq \lambda_0/2$, where λ_0 is the free-space wavelength, in order to excite the first higher order leaky mode. As shown in [12], the circular metallic rim is placed at a radial distance ρ_ap from the center so as to coincide with one of the zeros of the stationary Bessel distribution supported by the cavity. As opposed to the azimuthally invariant TM polarization analyzed in [12], in the HMD-fed case, there are different tangential electric field components that should be zero on the circular metallic rim. As mentioned in Section II, by correctly choosing the aperture radius of the structure, a radial resonance may or may not be enforced, and correspondingly, a TM-, TE-, or hybrid-polarized BB launcher can be achieved. For the TM polarization excited by an HMD, both E_z and E_ϕ follow the radial distribution of A_z [see (4e) and (4f)] whereas, for the TE polarization, there is only the tangential electric field component E_ϕ that is proportional to $\mathcal{C}_F'(\rho)$ [see (7b)]. Since in the HMD-fed launcher, there are both TM and TE contributions, we can choose to enforce the radial resonance for only one tangential electric field component (TM or TE) or none. In the latter case, neither the TM contribution nor the TE one is negligible, with respect to the other and thus, the complete analysis described in Section II is needed.

TABLE I
Parameters of the Designed BB Launchers

Parameter	TM	TE	Hybrid
X_s	26.21 Ω	41.20 Ω	32.86 Ω
h	6.38 mm	5.99 mm	6.18 mm
ρ_ap	17.19 mm	14.50 mm	16.50 mm
z_ndr	20.15 mm	20.11 mm	20.58 mm
$k_{\rho e}/k_0$	$0.6489 - j0.0025$	$0.6014 - j0.0067$	$0.6255 - j0.0041$
$k_{\rho h}/k_0$	$0.6379 - j0.0008$	$0.5849 - j0.0028$	$0.6120 - j0.0015$

As mentioned in Section II, the resonant contribution is dominant when the aperture-radius value is set to enforce a radial resonance between the outward and the inward cylindrical leaky waves, thus obtaining a stationary field distribution. The latter is totally described by the radial dependence $J_1(\cdot)$ of the field. By assuming that $\mathcal{C}_F(\rho) \propto J_1(k_{\rho h}\rho)$ and $\mathcal{C}_A(\rho) \propto J_1(k_{\rho e}\rho)$, the radial resonance of the TE or TM polarization can be achieved as follows:

$$\beta_h \rho_\mathrm{ap} = j_{1q}' \tag{20a}$$

$$\beta_e \rho_\mathrm{ap} = j_{1q} \tag{20b}$$

where j_{1q} is the qth zero of the first-order Bessel function and j_{1q}' is the qth zero of the first derivative of the first-order Bessel function. It is worthwhile noting that the argument of the first-order Bessel function is generally complex; however, we can enforce the radial resonance by considering only the real part related to β, due to the small values typically attained by α.

Following the design workflow of previous works (see, e.g., [14], [46]) in order to correctly design the BB launcher and choosing, e.g., $q = 2$, at the working frequency $f_0 = 30$ GHz, we get the TE and TM parameters in Table I. In particular, the values of β are obtained from (20a) and (20b), whereas those of α are set so as to maintain the

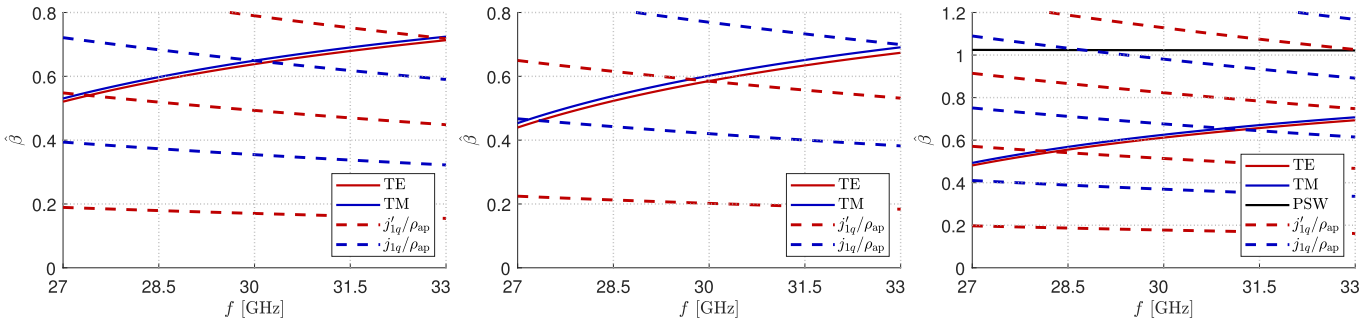

Fig. 2. Dispersion curves for the TM and TE leaky modes in the case of (a) TM, (b) TE, and (c) hybrid polarization of BB launchers whose design parameters are reported in Table I. Dashed lines represent the TM (blue line) and TE (red line) radial resonance of the structure, whereas solid lines show the dispersion curves of the phase constant of the higher order TM (blue line) and TE (red line) leaky modes of the TM PSW (black).

amplitude of the incident and reflected cylindrical leaky waves almost equal each other. The values of X_S and h are then easily derived from the knowledge of β and α as described in [47].

By numerically solving (12) with the values of $X_s = -1/B_s$, h and ρ_{ap} in Table I, the dispersion curves of the TM and TE first higher order leaky modes are found and reported as $\hat{\beta} = \beta/k_0$ versus frequency f in Fig. 2. As expected and shown in Fig. 2(a), there is a radial resonance of the TM field corresponding to the intersection, at the working frequency $f_0 = 30$ GHz, of the TM leaky-wave dispersion curve (blue solid line) and the hyperbolic blue dashed curve given by (20b) with $q = 2$ and ρ_{ap} as in Table I. The same analysis can be done in the TE case obtaining the radial resonance shown in Fig. 2(b) given by the intersection of the red solid and dashed lines that represent the TE leaky-wave dispersion curve and TE radial resonances (given by (20a), respectively.

In order to obtain a hybrid polarization, instead, we have to avoid all the TM or TE radial resonances at the working frequency. Moreover, in this nonresonant case, it is important to avoid also the radial resonances of the plasmonic surface wave (PSW) (see, e.g., [48]) in order not to have a dominant plasmonic field contribution (the effect of the PSW will be analyzed more in depth in future works). For a suitable choice of X_s, h, and ρ_{ap} (see the column "Hybrid" of Table I), the TM, TE, and PSW radial resonance can be avoided (the nondiffracting range reported in Table I in this case is conventionally computed by considering $\beta = \beta_e$). The validity of the proposed design can be inferred from the dispersion diagrams and the radial resonances in Fig. 2(c): there are no intersections between solid and dashed lines at the operating frequency and, therefore, there are no resonant modes.

As shown in [14], the maximum theoretical available bandwidth of a resonant TM launcher can be determined by the closest intersections with surface-wave or lower/higher leaky modes that surround the operating point. By the same token, a similar bandwidth can be defined for the TE case. Therefore, this bandwidth definition only holds for launchers that are either purely TM or purely TE (i.e., for devices excited by a VED- or VMD-like source). In the hybrid case, a very narrow bandwidth is achieved, limited by the TE and TM resonances, where the mode is hybrid and transitions from one polarization to the other as the frequency changes. However, the resonant character of these launchers usually leads to a very narrow impedance bandwidth. As a result, the operative bandwidth for each configuration (set by the minimum between the impedance and the maximum theoretical available bandwidths) can be defined by observing where the reflection coefficients are lower than a given threshold (typically $|S_{11}| < -10$ dB), but this mainly depends on the matching structure chosen for the feeder (see Section V).

The field distributions of the BB launchers designed above are those reported in Fig. 3. The amplitudes of E_x, E_y, E_z, and H_z are shown, on an xy plane at a fixed distance $z = z_{ndr}/2$ from the interface, whereas H_x and H_y are not represented for brevity because of their similarity to E_y and E_x, respectively.

While the figures labeled as "full wave" are obtained through a frequency-domain CST simulation of the entire 3-D structure, the field distributions labeled as "radiation integral" are obtained in a purely theoretical fashion. Starting from the field distributions derived in Section II, the surface equivalence theorem has been applied in order to find the equivalent magnetic and electric surface currents used as sources for radiation integrals [49]. In this manner, the field distribution obtained through radiation integrals can be compared to the simulated one in order to validate the theoretical analysis.

In particular, the full-wave and radiation-integral results for the TM-polarized BB launcher designed above are reported in Fig. 3(a)–(d) and (e)–(h), respectively. It is worthwhile to notice that H_z is negligible with respect to the other magnetic field components, as expected in a TM-polarized structure. Fig. 3(i)–(p) shows the full-wave and numerical results of the TE-polarized BB launcher. As opposed to the previous case, having a TE polarization, E_z is negligible with respect to the other electric field components, as shown in Fig. 3(k) and (o). For the hybrid-polarized case, the simulation results and the theoretical results obtained through radiation integral are reported in Fig. 3(q)–(t) and (u)–(x), respectively. In contrast to the previous cases, in the hybrid-polarized structure, there are no negligible components. Regardless of the polarization type, the full-wave results are very similar to the field distribution obtained through the numerical evaluation of the Huygens–Fresnel radiation integral. This comparison between full-wave and numerical results corroborates the consistency of the overall theoretical approach.

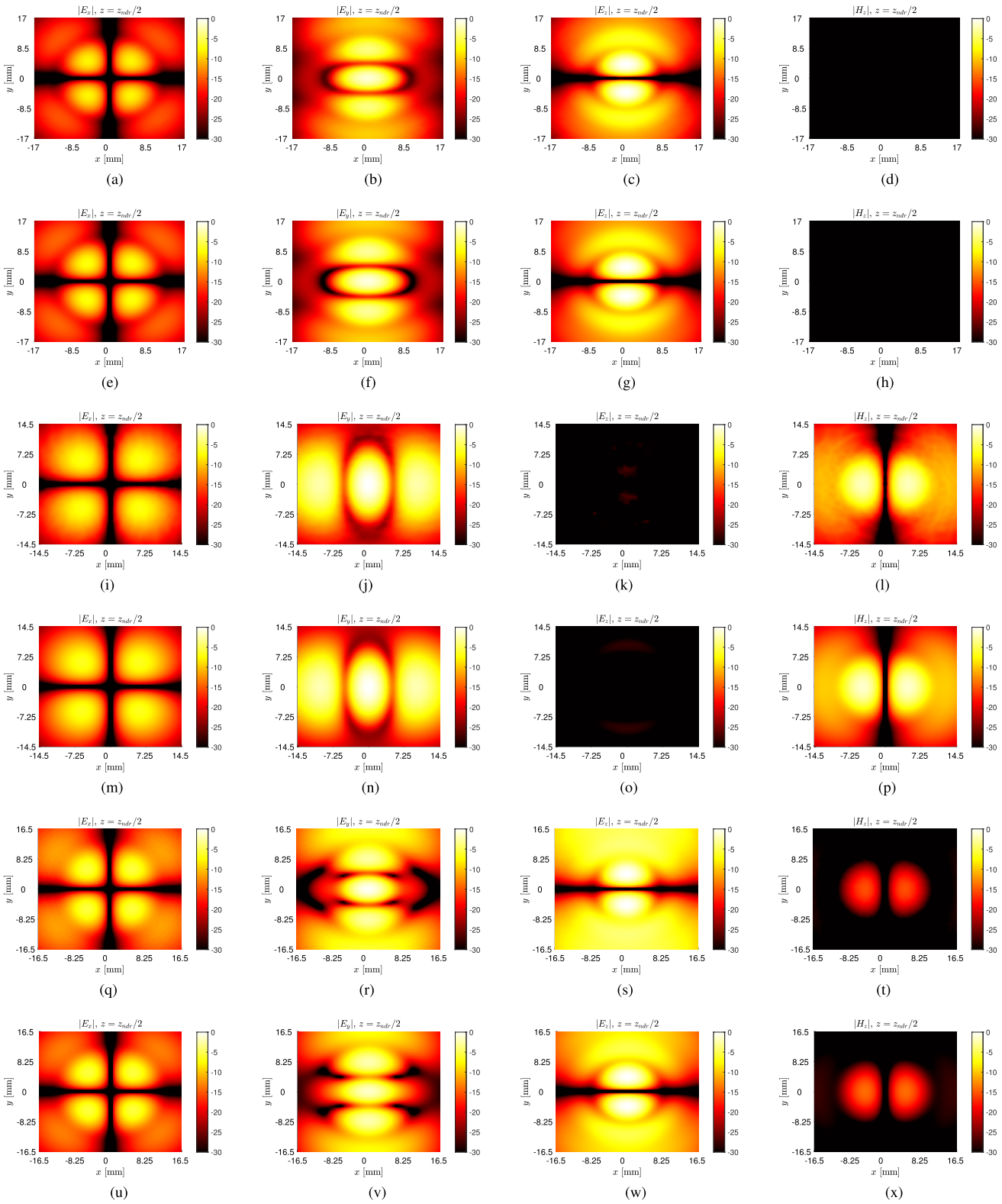

Fig. 3. Electric and magnetic field distributions over the xy plane, obtained through full-wave and radiation-integral results, for the BB launchers under analysis with TM, TE, and hybrid polarizations. All the components are normalized with respect to the maximum of their respective field at the $z = z_{\mathrm{ndr}}/2$ plane. (a)–(d) TM full wave. (e)–(h) TM radiation integral. (i)–(l) TE full wave. (m)–(p) TE radiation integral. (q)–(t) Hybrid full wave. (u)–(x) Hybrid radiation integral.

For the sake of brevity, in Fig. 4, we report only the E_x electric field component on the $\phi = 45°$, normalized with respect to its maximum, for each differently polarized BB launcher. The choice of this particular component and ϕ-plane is motivated by the following considerations. First, among all field components, E_x has a similar spatial distribution over the

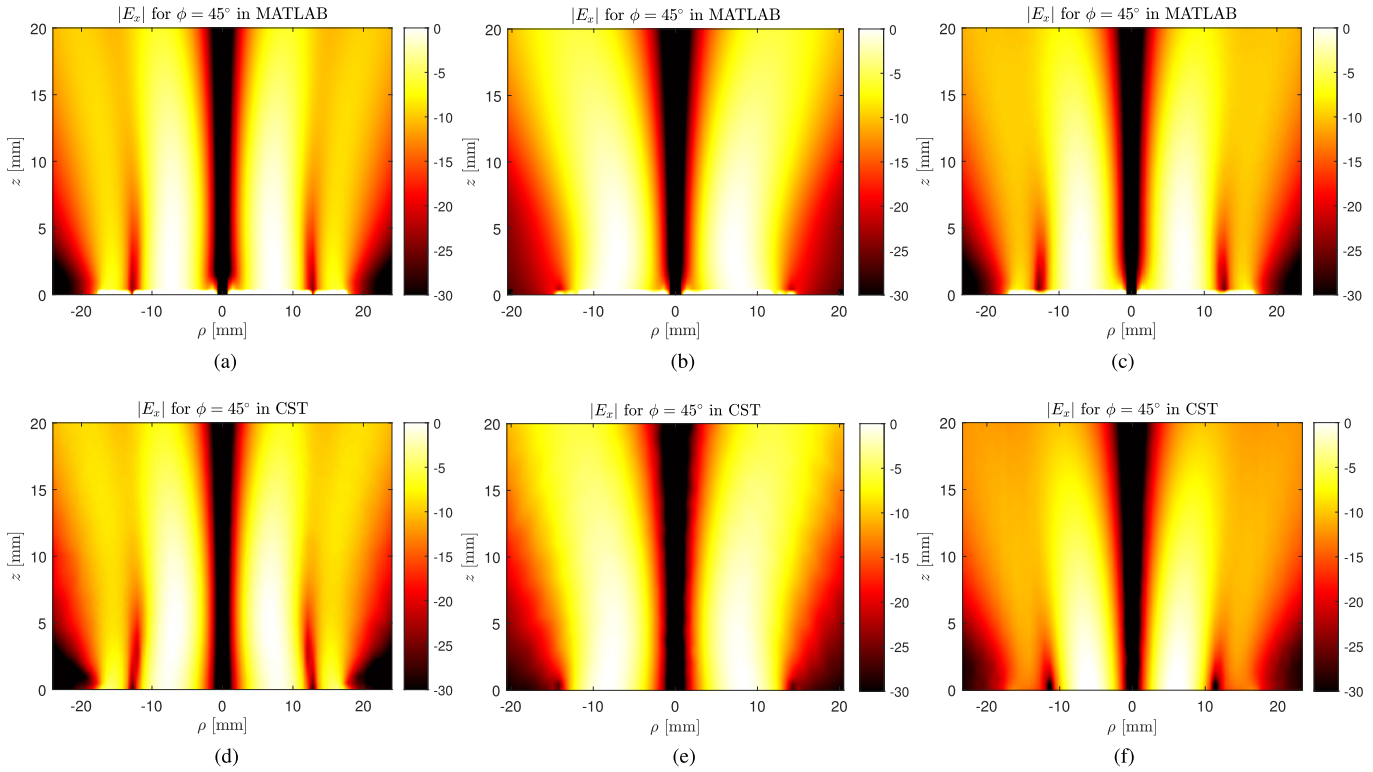

Fig. 4. E_x distributions on the $\phi = 45°$-plane for the BB launcher under analysis, in which each component is normalized to its maximum, obtained through (a)-(c) radiation-integral and (d)-(f) full-wave results. (a) and (d) $|E_x|$ for the TM-polarized BB launcher. (b) and (e) $|E_x|$ for the TE-polarized BB launcher. (c) and (f) $|E_x|$ for the hybrid-polarized BB launcher.

xy plane (see the fourfold symmetric patterns in Fig. 3) for all TM, TE, and hybrid polarizations. Second, the principal planes ($x = 0$ and $y = 0$) are symmetry planes for the field distribution where $E_x = 0$, whereas E_x is nonzero and symmetric with respect to $\phi = 45°$ and $\phi = -45°$. Given the longitudinal envelope of the field and the excellent agreement between full-wave and numerical results reported in Fig. 4, the limited diffraction of the beams and the consistency of the theoretical description are further confirmed.

V. Wireless Power Transfer

In this section, we perform a comparative study of WPT systems based on the aperture-fed BB launchers analyzed so far, exploiting the analytical framework developed in Section II. The result obtained for a radiative near-field WPT link is then compared with a typical example of a nonradiative near-field WPT link [50].

A. Near-Field WPT Link Through Aperture-Fed BB Launchers

The analysis and design of a WPT transmitter/receiver system working at around 30 GHz based on the radiative near-field coupling of two resonant BB launchers with VED feeders have recently been studied in [51]. Here, we analyze instead a WPT transmitter/receiver system consisting of two HMD-fed BB launchers in order to understand whether this kind of feeder is also suitable for realizing BB-WPT links. Full-wave results in a WPT scenario are then reported so as to compare the performance at microwave/millimeter-wave

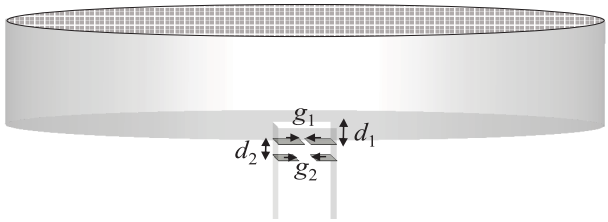

Fig. 5. Matching structure of a BB launcher excited by a waveguide-fed slot. Parameters provided in Tables II and III.

frequencies among TM, TE, and hybrid polarizations of the structure under analysis.

In order to obtain a consistent comparison among these WPT systems, we should obtain almost the same $|S_{11}|$ value for each polarization considering different working distances between the launchers. The hybrid-polarized BB launcher, due to its nonresonant nature, is considered as the starting case for the evaluation of the performance in terms of S_{11} and S_{21}. In order to correctly design the hybrid-polarized WPT system (Fig. 5), a good impedance matching of the launchers is realized at the working frequency $f_0 = 30$ GHz for the case in which the receiver is placed 2 cm (about the nondiffracting range at $f_0 = 30$ GHz) away from the transmitter. The structure is matched at the nondiffracting range because it is expected that such a matching condition remains adequate also for larger distances. For shorter distances, a different matching optimization should be done in each case of interest. The matching structure is constituted by two irises inside the feeding waveguide

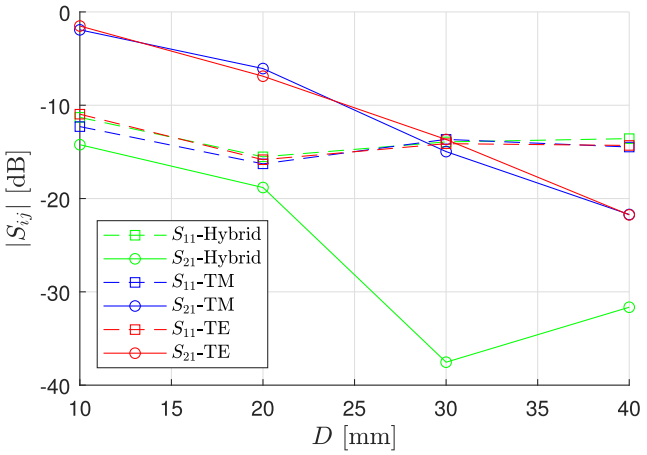

Fig. 6. Magnitude in dB of S_{11} (dashed lines) and S_{21} (solid lines) in a BB-WPT scenario is reported. Performance of differently polarized BB launchers is depicted with different colors: green for the hybrid-polarized link, blue for the TM case, and red for the TE case.

TABLE II
GEOMETRICAL PARAMETERS OF THE MATCHING IRISES FOR EACH DISTANCE BETWEEN TM-POLARIZED TRANSMITTER AND RECEIVER BB LAUNCHERS

D (mm)	d_1 (mm)	d_2 (mm)	g_1 (mm)	g_2 (mm)
10	0.83	4.96	0.15	1.08
20	0.69	4.59	0.13	1.11
30	0.66	4.18	0.13	1.07
40	0.66	4.18	0.12	1.07

TABLE III
GEOMETRICAL PARAMETERS OF THE MATCHING IRISES FOR EACH DISTANCE BETWEEN TE-POLARIZED TRANSMITTER AND RECEIVER BB LAUNCHERS

D (mm)	d_1 (mm)	d_2 (mm)	g_1 (mm)	g_2 (mm)
10	0.84	4.57	0.18	1.06
20	0.72	4.81	0.16	1.06
30	0.86	4.68	0.24	1.08
40	0.67	4.99	0.16	1.08

(see Fig. 5) whose geometrical parameters are: d_1, which represents the distance of the first iris from the slot on the ground plane, d_2, which is the distance of the second iris from the first one, and g_1 and g_2, which represent the gap sizes along the y-direction of the first and the second iris, respectively. By applying a full-wave optimization, we achieve the following geometrical parameters of the matching irises that minimize $|S_{11}|$ at f_0: $d_1 = 3.67$ mm, $d_2 = 0.10$ mm, $g_1 = 0.43$ mm, and $g_2 = 0.87$ mm. Once the device is fully designed, its WPT performance is evaluated in terms of S-parameters when the receiver is placed at a distance D of 10, 20, 30, or 40 mm (see green lines in Fig. 6).

In order to obtain a consistent comparison between the hybrid-, TE-, and TM-polarized WPT systems, we changed the geometrical parameters of the matching irises in the feeding waveguide in the TE and TM cases considering the receiver launcher placed at 10, 20, 30, or 40 mm, so as to obtain, at each distance, almost the same $|S_{11}|$ value of the hybrid-polarized case (see the dashed curves of Fig. 6). For each case, the full-wave optimization leads to the irises parameters reported in Tables II and III for the TM- and TE-polarized BB launcher designed in Section IV, respectively. However, we should stress here that the focus of the work is not on the impedance matching of the structures, which requires dedicated analyses that differ on a case-by-case basis. Here, we chose the simplest technique (i.e., matching irises in the waveguide case) that allowed us for obtaining a similar and satisfactory performance for all the polarizations of the BB launchers.

The results of this analysis for the S-parameters of the coupled BB launchers versus distance are reported in Fig. 6 with blue and red lines for the TM and TE case, respectively. The hybrid-polarized configuration shows almost the same $|S_{11}|$ (green dashed line) but also a much lower $|S_{21}|$ (green solid line) with respect to the TM- and TE-polarized cases. Interestingly, the hybrid-polarized BB launcher shows inferior performance and transmission efficiency with respect to the TM- and TE-polarized structures, although both modes are propagating. This is most likely due to the nonresonant nature of the hybrid case that strongly decreases the transmission efficiency and, in turn, the received power. In addition, it is noted (see Fig. 7) that the real part of the z-component of the Poynting vector on the xz plane is more focused in the case of a TM-polarized, slot-excited BB launcher with respect to the TE and hybrid case. The same consideration holds for the case of a TE-polarized, slot-excited BB launcher when observed on the yz plane (not shown for brevity), where we have the dual behavior of the Poynting vector for the TE and TM polarizations.

This effect reduces the diffractive spreading of the transmitted power outside the WPT system, thus increasing its radiation efficiency and decreasing the amount of wasted power. However, in the hybrid case, good coupling between transmitter and receiver is never achieved. While the hybrid-polarized case looks unsuitable for WPT applications, the HMD-fed BB launchers with TE or TM polarization show interesting properties of transmission efficiency and impedance matching, comparable with classical feeders such as coaxial cables or loop antennas [46]. In conclusion, our analysis shows that BB launchers excited with a waveguide-fed slot and designed in order to obtain a TE or TM polarization are promising candidates for future radiative near-field WPT applications at microwave and millimeter-wave frequencies. In Section V-B, a brief comparison between radiative near-field WPT links based on BBs and more conventional nonradiative near-field links is addressed.

B. Comparison Between Nonradiative and Radiative Near-Field WPT Links Based on BBs

In recent years, many works have dealt with the analysis and implementation of radiative near-field WPT links, but a quantitative comparison between radiative and nonradiative

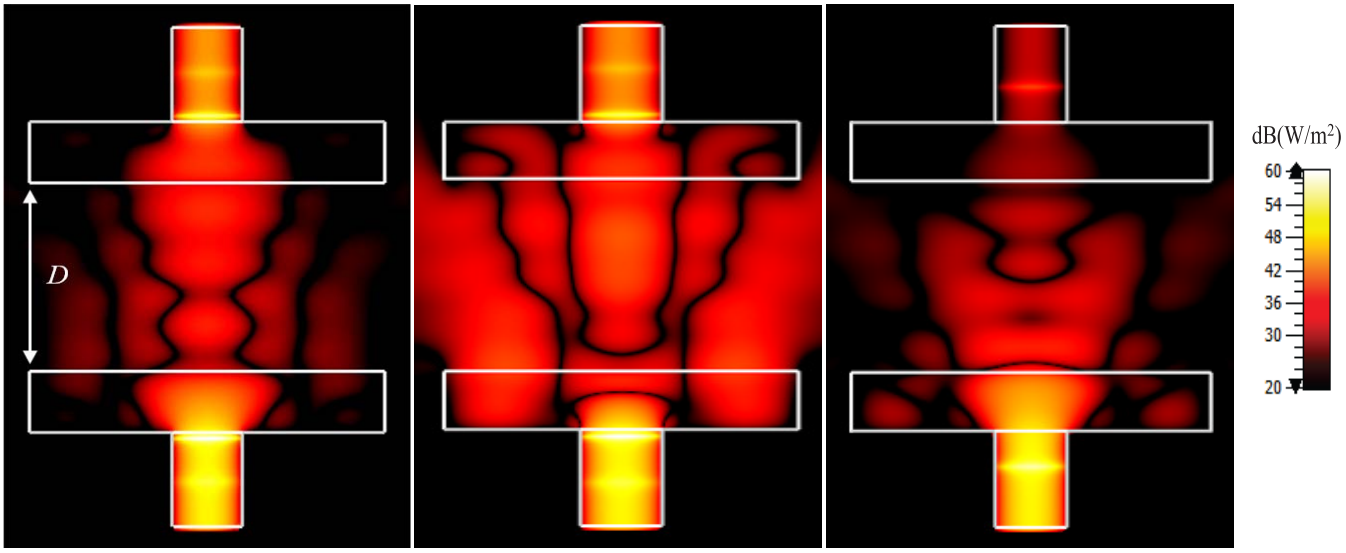

Fig. 7. WPT scenarios constituted by two identical BB launchers, excited by a waveguide-fed slot and placed at 20 mm in front of each other, designed in order to obtain (a) TM, (b) TE, and (c) hybrid polarization. On the xz plane, the z-component of the real part of the Poynting vector is reported as a contour plot.

near-field WPT links is still lacking. Gowda et al. [3] explained that, in the reactive near-field zone, power is transferred between resonant circuits via magnetoinductive coupling reaching high transmission efficiency. Their usage is, however, limited to small separation distances D between source and target since the efficiency of magnetoinductive systems fall off as $1/D^6$. As shown in [3], in nonradiative near-field links, there is also the issue of the strong coupling dependence on a resonance frequency, which shifts as the distance between the resonant circuits varies. Therefore, a method for either changing the operating frequency or dynamically retuning the resonators to maintain optimal efficiency is needed.

In order to obtain a fair comparison between radiative and nonradiative near-field links, it is necessary to design both structures in almost the same working condition. Due to the different field zones and radiation methods, however, it is not possible to consider exactly the same situation for both links. It is worthwhile to point out that the design of a BB launcher at a few megahertz frequencies (as in nonradiative links) would considerably increase in size, as it scales with the wavelength.

In [50], a comprehensive analysis and measurements are reported for a nonradiative WPT system. In particular, the authors considered a resonant shielded-loop link consisting of two coaxial, electrically small, loop antennas with a primarily magnetic response and radius set at $\rho_{\mathrm{l}} = 10.7$ cm. By following the design workflow briefly discussed in [46], BB launchers can be realized with the same aperture radius $\rho_{\mathrm{ap}} = \rho_{\mathrm{l}}$ and capable of reaching distances between the transmitter and the receiver compared to the cases analyzed in [50]. By considering, e.g., two aperture-fed TM-polarized BB launchers at the working frequencies $f_1 = 10$ GHz and at $f_2 = 7$ GHz, the design parameters of the two desired BB launchers are: $q_1 = q_2 = 2$, $\rho_{\mathrm{ap},1} = \rho_{\mathrm{ap},2} = \rho_{\mathrm{l}} = 10.7$ cm, $X_{\mathrm{S},1} = 15\ \Omega$, and $X_{\mathrm{S},2} = 20\ \Omega$. $h_1 = 15.57$ mm and $h_2 = 23.487$ mm. The simulated field distributions of these devices, not reported for brevity, have the same behavior shown in Fig. 3 on a wider area, further confirming the effectiveness of the theoretical analysis presented in Section II. The nondiffractive ranges are $z_{\mathrm{ndr},1} \simeq 32.5$ cm and $z_{\mathrm{ndr},2} \simeq 21.42$ cm. As can be inferred from Fig. 8, where $|S_{21}|^2$ is reported for this work and [50], the BB links have higher efficiency with respect to the nonradiative cases for very short distances and they maintain an almost constant and sufficient efficiency up to the nondiffractive range. $|S_{21}|^2$ shown by the links in [50] is instead generally higher than the one obtained through BB links, with very high peak values. However, in nonradiative links, there is also a high variability as the working distance changes, as expected.

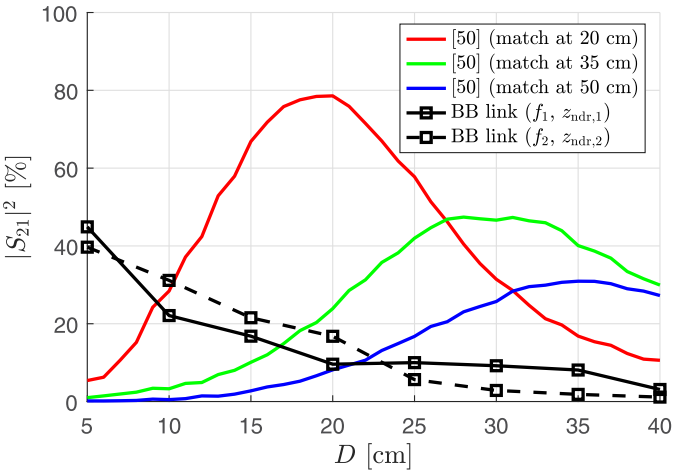

Fig. 8. Comparison between nonradiative WPT links and radiative near-field WPT links based on BBs with a fixed working frequency (represented through black solid and dashed lines for f_1 and f_2, respectively).

Note that the shielded loop works well in a very narrow bandwidth (see, e.g., [50, Fig. 5(b)]) of about $\Delta f = 8$ MHz, whereas the same frequency range is negligible for a BB launcher working at $f_1 = 10$ GHz or $f_2 = 7$ GHz. In order to achieve a fair comparison between different links,

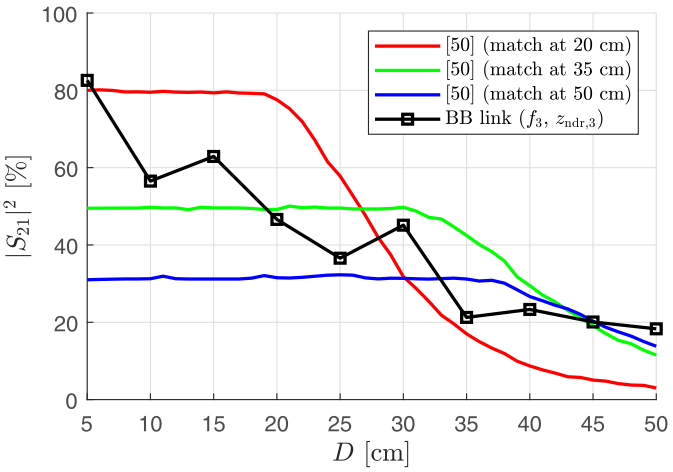

Fig. 9. Comparison among frequency-tuned nonradiative WPT links and radiative near-field WPT links based on BBs.

a tuned-frequency link with the same FBW for both BB launchers and shielded loops can be considered. In particular, the aforementioned bandwidth of the nonradiative link on a working frequency $f_1 = 38$ MHz leads to FBW $\simeq 20\%$. As commented above, a BB launcher can be designed in order to be able to work with the same aperture radius $\rho_{\mathrm{ap},3} = \rho_1$ and to reach a distance between transmitter and receiver comparable with the cases analyzed in [50]. In this case, an aperture-fed TM-polarized BB launcher at the working frequency $f_3 = 20$ GHz (thus, with $\Delta f_{\mathrm{BBL}} \simeq 4$ GHz) has been considered with the following design parameters: $q_3 = 4$, $\rho_{\mathrm{ap},3} = 10.7$ cm, $X_{\mathrm{S},3} = 25\ \Omega$, and $h_3 = 7.676$ mm. The nondiffractive range is $z_{\mathrm{ndr},3} \simeq 34.42$ cm that is similar to the distances analyzed in [50].

The WPT results are shown in Fig. 9 where $|S_{21}|^2$ is reported for this work and the different cases analyzed in [50], in a frequency-tuned scenario with the same FBW. The BB link shows a better performance for larger distances with respect to the network optimized at 20 cm in [50] (as expected for a radiative near-field link with respect to a nonradiative one). In the other two cases, the BB link has everywhere a better performance than the nonradiative near-field links except for a narrow area centered at the points in which the nonradiative links are optimized. Note that these comparisons are made by considering a single structure for the BB launcher, whereas the three links analyzed in [50] are realized through three different architectures.

VI. Conclusion

In this work, we have developed a theoretical framework based on an effective leaky-wave approach to obtain an approximate still accurate analytical description of the fields radiated in the near-field region by a BB launcher excited through an HMD, which is then realized with a waveguide-fed slot etched in the ground plane. In particular, by choosing the aperture radius, a TM, TE, or hybrid polarization can be achieved. Analytical and numerical results are then compared with full-wave simulations obtaining an excellent agreement in all the differently polarized BB launchers.

A numerical evaluation of the field, obtained by this simple theoretical approach, can be useful for further studies on this kind of BB launchers and their performance in different application scenarios as shown, for example, in WPT links. We have observed that a BB launcher excited by an HMD shows interesting performance in WPT scenarios.

Differently polarized BB launchers show, however, different performances. While TM- and TE-polarized BB launchers have comparable and interesting efficiency in a typical WPT scenario, the hybrid-polarized structure shows a lower value due to the nonresonant nature of the device. The investigation of resonant hybrid-polarized launchers, necessarily based on structures different from those considered in this work, will be the subject of future investigations.

In addition, we performed a quantitative comparison between radiative and nonradiative WPT links that was previously missing in the available literature. In particular, it is shown that radiative WPT links based on BBs achieve a higher resilience to changes in distance and frequency with respect to nonradiative WPT links based on shielded loops. Nonetheless, the typical reactive near-field link, however, generally achieves higher efficiency. In a frequency-tuned scenario, instead, the links based on BBs show better performance than the nonradiative cases. In conclusion, BBs can be considered important candidates in the implementation of future WPT links at microwave and millimeter-wave frequencies.

References

[1] M. Wagih, A. S. Weddell, and S. Beeby, "Millimeter-wave power harvesting: A review," *IEEE Open J. Antennas Propag.*, vol. 1, pp. 560–578, 2020.

[2] J. Zhou, P. Zhang, J. Han, L. Li, and Y. Huang, "Metamaterials and metasurfaces for wireless power transfer and energy harvesting," *Proc. IEEE*, vol. 110, no. 1, pp. 31–55, Jan. 2022.

[3] V. R. Gowda, O. Yurduseven, G. Lipworth, T. Zupan, M. S. Reynolds, and D. R. Smith, "Wireless power transfer in the radiative near field," *IEEE Antennas Wireless Propag. Lett.*, vol. 15, pp. 1865–1868, 2016.

[4] J. D. Heebl, M. Ettorre, and A. Grbic, "Wireless links in the radiative near field via Bessel beams," *Phys. Rev. A, Gen. Phys.*, vol. 6, no. 3, Sep. 2016, Art. no. 034018.

[5] H. E. Hernández-Figueroa, M. Zamboni-Rached, and E. Recami, *Nondiffracting Waves*. Weinheim, Germany: Wiley, 2013.

[6] H. E. Hernández-Figueroa, M. Zamboni-Rached, and E. Recami, *Localized Waves*. Hoboken, NJ, USA: Wiley, 2007.

[7] M. Yessenov, B. Bhaduri, H. E. Kondakci, and A. F. Abouraddy, "Classification of propagation-invariant space-time wave packets in free space: Theory and experiments," *Phys. Rev. A, Gen. Phys.*, vol. 99, no. 2, Feb. 2019, Art. no. 023856.

[8] J. Durnin, "Exact solutions for nondiffracting beams. I. The scalar theory," *J. Opt. Soc. Amer. A, Opt. Image Sci.*, vol. 4, no. 4, pp. 651–654, 1987.

[9] J. Durnin, J. J. Miceli, and J. H. Eberly, "Diffraction-free beams," *Phys. Rev. Lett.*, vol. 58, no. 15, p. 1499, 1987.

[10] D. Comite, W. Fuscaldo, P. Burghignoli, A. Galli, and P. Baccarelli, "Bessel-beam antennas," in *Wiley Encyclopedia of Electrical and Electronics Engineering*, J. Webster, Ed. New York, NY, USA: Wiley, 2021, pp. 1–12.

[11] M. Ettorre, S. C. Pavone, M. Casaletti, M. Albani, A. Mazzinghi, and A. Freni, "Near-field focusing by non-diffracting Bessel beams," in *Aperture Antennas for Millimeter and Sub-Millimeter Wave Applications*. Cham, Switzerland: Springer, 2018, pp. 243–288.

[12] M. Ettorre and A. Grbic, "Generation of propagating Bessel beams using leaky-wave modes," *IEEE Trans. Antennas Propag.*, vol. 60, no. 8, pp. 3605–3613, Aug. 2012.

[13] M. Ettorre, S. M. Rudolph, and A. Grbic, "Generation of propagating Bessel beams using leaky-wave modes: Experimental validation," *IEEE Trans. Antennas Propag.*, vol. 60, no. 6, pp. 2645–2653, Jun. 2012.

[14] W. Fuscaldo, G. Valerio, A. Galli, R. Sauleau, A. Grbic, and M. Ettorre, "Higher-order leaky-mode Bessel-beam launcher," *IEEE Trans. Antennas Propag.*, vol. 64, no. 3, pp. 904–913, Mar. 2016.

[15] M. Ettorre et al., "On the near-field shaping and focusing capability of a radial line slot array," *IEEE Trans. Antennas Propag.*, vol. 62, no. 4, pp. 1991–1999, Apr. 2014.

[16] S. C. Pavone, M. Ettorre, and M. Albani, "Analysis and design of Bessel beam launchers: Longitudinal polarization," *IEEE Trans. Antennas Propag.*, vol. 64, no. 6, pp. 2311–2318, Jun. 2016.

[17] S. C. Pavone, M. Ettorre, M. Casaletti, and M. Albani, "Transverse circular-polarized Bessel beam generation by inward cylindrical aperture distribution," *Opt. Exp.*, vol. 24, no. 10, pp. 11103–11111, 2016.

[18] D. Comite et al., "Radially periodic leaky-wave antenna for Bessel beam generation over a wide-frequency range," *IEEE Trans. Antennas Propag.*, vol. 66, no. 6, pp. 2828–2843, Jun. 2018.

[19] P. Lemaitre-Auger, S. Abielmona, and C. Caloz, "Generation of Bessel beams by two-dimensional antenna arrays using sub-sampled distributions," *IEEE Trans. Antennas Propag.*, vol. 61, no. 4, pp. 1838–1849, Apr. 2013.

[20] N. Chiotellis, V. Mendez, S. M. Rudolph, and A. Grbic, "Experimental demonstration of highly localized pulses (X waves) at microwave frequencies," *Phys. Rev. B, Condens. Matter*, vol. 97, no. 8, Feb. 2018, Art. no. 085136.

[21] N. Chiotellis, S. Zhang, Y. C. Vardaxoglou, and A. Grbic, "X wave radiator implemented with 3-D printed metamaterials," *IEEE Trans. Antennas Propag.*, vol. 68, no. 7, pp. 5478–5486, Jul. 2020.

[22] M. Q. Qi, W. X. Tang, and T. J. Cui, "A broadband Bessel beam launcher using metamaterial lens," *Sci. Rep.*, vol. 5, no. 1, p. 11732, Dec. 2015.

[23] S. Pakovic, N. Bartolomei, M. J. Mencagli, M. Ettorre, R. Sauleau, and D. Gonzalez-Ovejero, "A fast and accurate method of synthesizing X-wave launchers by metallic horns," *IEEE Access*, vol. 9, pp. 1996–2006, 2021.

[24] S. Paković, S. Zhou, D. González-Ovejero, S. C. Pavone, A. Grbic, and M. Ettorre, "Bessel–Gauss beam launchers for wireless power transfer," *IEEE Open J. Antennas Propag.*, vol. 2, pp. 654–663, 2021.

[25] P. Lu, A. Breard, J. Huillery, X.-S. Yang, and D. Voyer, "Feeding coils design for TE-polarized Bessel antenna to generate rotationally symmetric magnetic field distribution," *IEEE Antennas Wireless Propag. Lett.*, vol. 17, no. 12, pp. 2424–2428, Dec. 2018.

[26] P. Lu et al., "Design of TE-polarized Bessel antenna in microwave range using leaky-wave modes," *IEEE Trans. Antennas Propag.*, vol. 66, no. 1, pp. 32–41, Jan. 2017.

[27] E. S. G. Rodríguez, M. Machnoor, and G. Lazzi, "On the generation of nondiffracting beams in extremely subwavelength applications," *IEEE Trans. Antennas Propag.*, vol. 65, no. 10, pp. 5228–5237, Oct. 2017.

[28] A. Omar, R. Caverly, W. Doherty, R. Watkins, A. Gopinath, and J. T. Vaughan, "A microwave engineer's view of MRI," *IEEE Microw. Mag.*, vol. 12, no. 3, pp. 78–86, May 2011.

[29] Y. F. Wu, Y. J. Cheng, Y. C. Zhong, and H. N. Yang, "Substrate integrated waveguide slot array antenna to generate Bessel beam with high transverse linear polarization purity," *IEEE Trans. Antennas Propag.*, vol. 70, no. 1, pp. 750–755, Jan. 2022.

[30] Y. F. Wu and Y. J. Cheng, "Two-dimensional near-field focusing folded reversely fed leaky-wave antenna array with high radiation efficiency," *IEEE Trans. Antennas Propag.*, vol. 67, no. 7, pp. 4560–4569, Jul. 2019.

[31] D. M. Sheen, D. L. McMakin, and T. E. Hall, "Three-dimensional millimeter-wave imaging for concealed weapon detection," *IEEE Trans. Microw. Theory Techn.*, vol. 49, no. 9, pp. 1581–1592, Sep. 2001.

[32] Z. Bouchal and M. Olivík, "Non-diffractive vector Bessel beam," *J. Mod. Opt.*, vol. 42, no. 8, pp. 1555–1566, Aug. 1995.

[33] Y. Monnai, D. Jahn, W. Withayachumnankul, M. Koch, and H. Shinoda, "Terahertz plasmonic Bessel beamformer," *Appl. Phys. Lett.*, vol. 106, no. 2, Jan. 2015, Art. no. 021101.

[34] P. Burghignoli, W. Fuscaldo, and A. Galli, "Fabry–Perot cavity antennas: The leaky-wave perspective," *IEEE Antennas Propag. Mag.*, vol. 63, no. 4, pp. 116–145, Aug. 2021.

[35] A. Ip and D. R. Jackson, "Radiation from cylindrical leaky waves," *IEEE Trans. Antennas Propag.*, vol. 38, no. 4, pp. 482–488, Apr. 1990.

[36] P. Burghignoli, W. Fuscaldo, D. Comite, P. Baccarelli, and A. Galli, "Higher-order cylindrical leaky waves—Part I: Canonical sources and radiation formulas," *IEEE Trans. Antennas Propag.*, vol. 67, no. 11, pp. 6735–6747, Nov. 2019.

[37] P. Burghignoli, D. Comite, W. Fuscaldo, P. Baccarelli, and A. Galli, "Higher-order cylindrical leaky waves—Part II: Circular array design and validations," *IEEE Trans. Antennas Propag.*, vol. 67, no. 11, pp. 6748–6760, Nov. 2019.

[38] O. C. Vicente and C. Caloz, "Bessel beams: A unified and extended perspective," *Optica*, vol. 8, no. 4, pp. 451–457, Apr. 2021.

[39] W. Fuscaldo, D. Comite, A. Boesso, P. Baccarelli, P. Burghignoli, and A. Galli, "Focusing leaky waves: A class of electromagnetic localized waves with complex spectra," *Phys. Rev. A, Gen. Phys.*, vol. 9, no. 5, 2018, Art. no. 054005.

[40] W. Fuscaldo, A. Benedetti, D. Comite, P. Baccarelli, P. Burghignoli, and A. Galli, "Bessel–Gauss beams through leaky waves: Focusing and diffractive properties," *Phys. Rev. A, Gen. Phys.*, vol. 13, no. 6, Jun. 2020, Art. no. 064040.

[41] G. Lovat, P. Burghignoli, and D. R. Jackson, "Fundamental properties and optimization of broadside radiation from uniform leaky-wave antennas," *IEEE Trans. Antennas Propag.*, vol. 54, no. 5, pp. 1442–1452, May 2006.

[42] (2019). *CST Products Darmstadt*. Germany. [Online]. Available: http://www.cst.com

[43] R. E. Collin, *Field Theory Guided Waves*. New York, NY, USA: Wiley, 1990.

[44] W. Fuscaldo et al., "Systematic design of THz leaky-wave antennas based on homogenized metasurfaces," *IEEE Trans. Antennas Propag.*, vol. 66, no. 3, pp. 1169–1178, Mar. 2018.

[45] O. Luukkonen et al., "Simple and accurate analytical model of planar grids and high-impedance surfaces comprising metal strips or patches," *IEEE Trans. Antennas Propag.*, vol. 56, no. 6, pp. 1624–1632, Jun. 2008.

[46] F. Benassi et al., "Comparison between hybrid- and TM-polarized Bessel-beam launchers for wireless power transfer in the radiative near-field at millimeter waves," in *Proc. 51st Eur. Microw. Conf. (EuMC)*, London, U.K., Apr. 2022, pp. 1–4.

[47] W. Fuscaldo, A. Galli, and D. R. Jackson, "Optimization of 1-D unidirectional leaky-wave antennas based on partially reflecting surfaces," *IEEE Trans. Antennas Propag.*, vol. 70, no. 9, pp. 7853–7868, Sep. 2022.

[48] E. Negri, W. Fuscaldo, M. Ettorre, P. Burghignoli, and A. Galli, "Analysis of resonant Bessel-beam launchers based on isotropic metasurfaces," in *Proc. 16th Eur. Conf. Antennas Propag. (EuCAP)*, Madrid, Spain, Mar./Apr. 2022, pp. 1–4.

[49] C. A. Balanis, *Advanced Engineering Electromagnetics*. Hoboken, NJ, USA: Wiley, 2012.

[50] J. D. Heebl, E. M. Thomas, R. P. Penno, and A. Grbic, "Comprehensive analysis and measurement of frequency-tuned and impedance-tuned wireless non-radiative power-transfer systems," *IEEE Antennas Propag. Mag.*, vol. 56, no. 4, pp. 44–60, Aug. 2014.

[51] F. Benassi, W. Fuscaldo, D. Masotti, A. Galli, and A. Costanzo, "Wireless power transfer in the radiative near-field through resonant Bessel-beam launchers at millimeter waves," in *Proc. IEEE Wireless Power Transf. Conf. (WPTC)*, San Diego, CA, USA, Jun. 2021, pp. 1–4.

Edoardo Negri (Graduate Student Member, IEEE) was born in Orvieto, Italy, in 1997. He received the B.Sc. and M.Sc. degrees (cum laude) in electronic engineering, with honorable mention for the academic curriculum, from the Sapienza University of Rome, Rome, Italy, in July 2019 and 2021, respectively, where he is currently pursuing the Ph.D. degree in information and communications technologies (applied electromagnetics curriculum).

His main research interests are leaky waves, metasurfaces, focusing devices, and wireless power transfer for high-frequency applications (ranging from microwaves to terahertz).

Mr. Negri received the "Antonio Ventura" Award as one of the best engineering students at the Sapienza University of Rome in 2022.

Walter Fuscaldo (Senior Member, IEEE) received the B.Sc. and M.Sc. (cum laude) degrees in telecommunications engineering from the Sapienza University of Rome, Rome, Italy, in 2010 and 2013, respectively, and the Ph.D. degree (cum laude and with the *Doctor Europaeus* label) in information and communication technology (applied electromagnetics curriculum) from the Department of Information Engineering, Electronics and Telecommunications (DIET) and the Institut d'Électronique et de Télécommunications de Rennes (IETR), Université de Rennes 1, Rennes, France, in 2017, under a cotutelle agreement between the institutions.

In 2014, 2017, and 2018, he was a Visiting Researcher with the NATO-STO Center for Maritime Research and Experimentation, La Spezia, Italy. In 2016, he was a Visiting Researcher with the University of Houston, Houston, TX, USA. Since July 2017, he was a Post-Doctoral Researcher with the Sapienza University of Rome. In July 2020, he joined the Institute for Microelectronics and Microsystems (IMM), National Research Council of Italy, Rome, as a Researcher. His current research interests include propagation of leaky waves, surface waves and plasmonic waves, analysis and design of leaky-wave antennas, generation of localized electromagnetic waves, graphene electromagnetics, metasurfaces, and terahertz antennas.

Dr. Fuscaldo was awarded several prizes, among which the prestigious Young Engineer Prize for the Best Paper presented at the 46th European Microwave Conference in 2016 and the Best Paper in Electromagnetics and Antenna Theory at the 12th European Conference on Antennas and Propagation in 2018. He was also awarded the IEEE Reviewer Certificate for excellent performance for the IEEE TRANSACTIONS ON ANTENNAS AND PROPAGATION journal in 2019, 2020, and 2021. He is currently an Associate Editor of the *IET Microwaves, Antennas and Propagation* journal and *IET Electronic Letters* and a Topic Editor of *MDPI Crystals* journal.

Paolo Burghignoli (Senior Member, IEEE) was born in Rome, Italy, in February 1973. He received the Laurea degree (cum laude) in electronic engineering and the Ph.D. degree in applied electromagnetics from the "La Sapienza" University of Rome, Rome, Italy, in 1997 and 2001, respectively.

In 1997, he joined the Department of Electronic Engineering, Sapienza University of Rome, where he is currently with the Department of Information Engineering, Electronics and Telecommunications. In 2004, he was a Visiting Research Assistant Professor with the University of Houston, Houston, TX, USA. From 2010 to 2015, he was an Assistant Professor with the Sapienza University of Rome, where he has been an Associate Professor since 2015. In 2017, he received the National Scientific Qualification for the role of a Full Professor of electromagnetic fields at Italian universities. He is currently teaching courses in electromagnetic fields, advanced antenna engineering, and analytical techniques for wave phenomena for the B.Sc., M.Sc., and Ph.D. programs in the information and communication technology (ICT) area with the Sapienza University of Rome. He has authored about 250 papers in international journals, books, and conference proceedings. His research interests include the analysis and design of planar antennas and arrays, leakage phenomena in uniform and periodic structures, numerical methods for integral equations and periodic structures, propagation and radiation in metamaterials, electromagnetic shielding, transient electromagnetics, and graphene electromagnetics.

Dr. Burghignoli was the Secretary of the 12th European Microwave Week in 2009 and a member of the Scientific Board and the Local Organizing Committee of the 41st Photonics and Electromagnetics Research Symposium in 2019. He was a recipient of the "Giorgio Barzilai" Laurea Prize (1996–1997) presented by the former IEEE Central and South Italy Section, the 2003 IEEE Microwave Theory and Techniques Society (MTT-S) Graduate Fellowship, and the 2005 Raj Mittra Travel Grant for junior researchers presented at the IEEE AP-S Symposium on Antennas and Propagation, Washington, DC, USA. In 2016 and 2020, the IEEE Antennas and Propagation Society recognized him as an Outstanding Reviewer of the IEEE TRANSACTIONS ON ANTENNAS AND PROPAGATION. He is currently an Associate Editor of *Electronics Letters* (Institution of Engineering and Technology) and the *International Journal of Antennas and Propagation* (Hindawi).

Alessandro Galli (Member, IEEE) received the Laurea degree in electronics engineering and the Ph.D. degree in applied electromagnetics from the Sapienza University of Rome, Rome, Italy, in 1990 and 1994, respectively.

Since 1990, he has been with the Department of Information Engineering, Electronics and Telecommunications, Sapienza University of Rome, where he became an Assistant Professor and an Associate Professor in the sector of electromagnetic fields in 2000 and 2002, respectively. In 2013, he passed the National Scientific Qualification, and in 2020, he definitively achieved the role of Full Professor in the same sector. He is currently teaching or co-teaching courses on electromagnetic fields, advanced antenna engineering, microwaves, and engineering electromagnetics. He has authored more than 300 papers in international journals, books, and conference proceedings. He holds a patent for an invention of a leaky-wave antenna. His research interests include electromagnetic guided-wave and radiation theory and applications ranging from microwaves to terahertz. Specific topics include leaky waves and leaky-wave antennas, periodic and multilayered printed structures, beam focusing devices, and complex media and metamaterials. His research activities have also included topics in geoelectromagnetics, bioelectromagnetics, and plasma heating.

Dr. Galli is a member of the leading scientific societies of electromagnetics. He was a recipient of various grants and prizes for his research activity, such as the Barzilai Prize for the best scientific work of under-35 researchers from the 10th National Meeting of Electromagnetics in 1994 and the Quality Presentation Recognition Award of the International Microwave Symposium by the IEEE Microwave Theory and Techniques Society in 1994 and 1995. In 2017, he has been elected as the Best Teacher of the courses of the European School of Antennas (ESoA). He is also an associate editor of two international journals on microwaves, antennas, and propagation. He was elected as the Italian Representative on the Board of Directors of the European Microwave Association (EuMA) for the 2010–2012 and 2013–2015 triennium. He was the General Co-Chair of the 2014 European Microwave Week, the most important conference event in the electromagnetic area at the European level. Since its foundation in 2012, he has been the Coordinator of the European Courses on Microwaves (EuCoM), the first European educational institution on microwaves.

Open Access funding provided by 'Università degli Studi di Roma "La Sapienza"' within the CRUI CARE Agreement